VIP Photothermal Therapy Very Important Paper

International Edition: DOI: 10.1002/anie.201605241
German Edition: DOI: 10.1002/ange.201605241

Controlling Spatial Heat and Light Distribution by Using Photothermal Enhancing Auto-Regulated Liposomes (PEARLs)

*Kenneth K. Ng, Robert A. Weersink, Liang Lim, Brian C. Wilson, and Gang Zheng**

Abstract: *Photothermal therapy (PTT) is enhanced by the use of nanoparticles with a large optical absorption at the treatment wavelength. However, this comes at the cost of higher light attenuation that results in reduced depth of heating as well as larger thermal gradients, leading to potential over- and under-treatment in the target tissue. These limitations can be overcome by using photothermal enhancing auto-regulating liposomes (PEARLs), based on thermochromic J-aggregate forming dye–lipid conjugates that reversibly alter their absorption above a predefined lipid phase-transition temperature. Under irradiation by near-infrared light, deeper layers of the target tissue revert to the intrinsic optical absorption, halting the temperature rise and enabling greater light penetration and heat generation at depth. This effect is demonstrated in both nanoparticle solutions and in gel phantoms containing the nanoparticles.*

The photothermal effect, whereby a photo-excited chromophore generates heat through non-radiative relaxation, has been studied in a variety of applications including solar-energy conversion, photoacoustic imaging/spectroscopy, actuation of nano- and micro-devices,[1] water desalination,[2] and chemical distillation.[3] In nanomedicine, enhancement of the photothermal effect over that intrinsic to tissues through the use of organic or inorganic nanoparticles (NPs) has been investigated for triggering drug release,[4] activation of targeting molecules,[5] and as a mechanism to generate heat in photothermal therapy.[6]

Specifically in the design of nanoparticles for photothermal therapy (PTT) of cancer, strong absorption at near-infrared (NIR) wavelengths is desired, since this minimizes light absorption by endogenous absorbers in tissue, while maximizing temperature generation mediated by the tumor-specific accumulation of nanoparticles. However, NPs that are dispersed homogenously throughout the target tissue volume will also increase the light attenuation (which is a combination of absorption and elastic scattering),[7] so that the deeper lying tissues will be exposed to lower light intensity and either take longer or fail to reach the desired temperature sufficient for hyperthermia or coagulative necrosis. This effect then imposes limits on the treatment volume. Hence, there is a significant trade-off required between the nanoparticle concentration, treatment time and light irradiance to ensure that effective treatment is delivered to the full target tissue thickness in a clinically-practical time and using affordable light sources, while avoiding overheating nearer the surface that can be hazardous to the patient and further limits the light penetration if charring occurs. Current strategies to address this challenge are largely based on modifications to the light-delivery, such as water-cooled fiber-optic sheaths for interstitial PTT,[8] the use of image guidance[9] and/or feedback control through on-line thermometry.[10]

J-aggregates (JAG) are formed from the coherent coupling of dyes to form a structure with ensemble optical properties.[11] Given the close distance and conformational requirements, JAGs are highly susceptible to changes in their surrounding environment. Using this principle, we previously demonstrated that J-aggregation of planar bacteriopheophorbide-lipid dyes in lipid nanoparticles display changes in absorption spectrum depending on whether the ambient temperature is lower or higher than the phase transition temperature of the nanoparticle. Monitoring this change using photoacoustic imaging enables spatial monitoring of temperature in real-time.[12] Since these nanoparticles generate sufficient absorption and thermal energy for photoacoustic imaging,[13] we asked whether these particles could be used as heat enhancers in photothermal therapy and whether their thermochromic behavior enables control of light propagation and closed loop regulation of photothermal heating.

Herein, we show that JAG-forming liposomes possessing photothermal feedback control can be used to regulate light transmission and photothermal heating with a pre-defined temperature set-point. These nanoparticles, which we coined photothermal enhancing auto-regulated liposomes (PEARL), utilize conformation-dependent absorption to drive photothermal conversion. In this particular application, we utilize J-aggregation between lipid-conjugated dyes formed within a thermoresponsive molecular environment. By linking the absorption state of the photothermal chromophore to a temperature-responsive host lipid, a feedback heating mechanism can be generated to sequentially increase light penetration and regulate temperature (Figure 1).

PEARLs are composed of 15 mol% bacteriopheophorbide-lipid dye conjugates dispersed in a thermoresponsive lipid bilayer (80 mol% dipalmitoylphosphatidylcholine (DPPC) and 5 mol% methoxy-PEG_{2000}-lipid). Extrusion of these lipids results in nearly monodispersed NPs with an average diameter of approximately 90 nm (Figure S1 in the

[*] Dr. K. K. Ng, Dr. R. A. Weersink, Dr. L. Lim, Prof. B. C. Wilson, Prof. G. Zheng
Princess Margaret Cancer Centre and TECHNA Institute
University Health Network
Toronto, ON, M5G 1L7 (Canada)
E-mail: gang.zheng@uhnres.utoronto.ca
Prof. B. C. Wilson, Prof. G. Zheng
Department of Medical Biophysics
University of Toronto
Ontario M5G 1L7 (Canada)

Supporting information for this article can be found under: http://dx.doi.org/10.1002/anie.201605241.

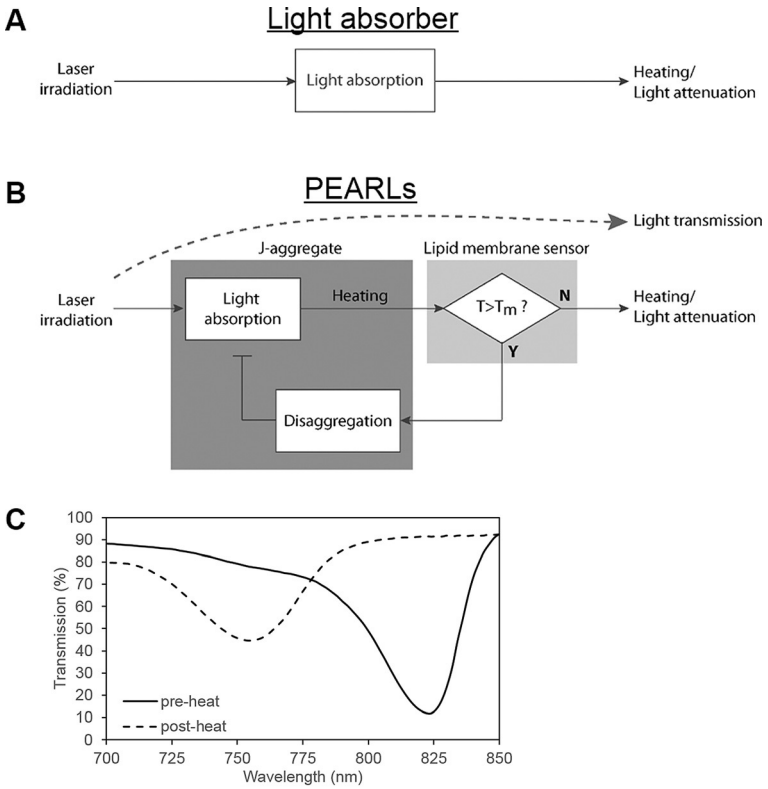

Figure 1. Schematic illustration of photothermal heating in two homogeneously dispersed absorber systems. A) With the traditional (molecular or nanoparticle) light absorber, laser illumination is converted into heat energy through the photothermal effect. Attenuation of light occurs as a consequence of the Beer–Lambert Law. B) In the photothermal enhancing auto-regulated liposome (PEARLs) system, laser illumination is converted into heat energy through the photothermal effect. The temperature increase is checked by the lipid-membrane sensor. Temperature increase above the phase transition set-point of the sensor induces a phase change, resulting in disruption of J-aggregate and inhibition of light absorption. This change enhances light transmission and regulates heat generation. C) Representative spectra of light transmission from PEARLs before and after photothermal heating above its temperature set-point.

Supporting Information). The 75 nm red shift to 824 nm puts the main absorption well within the near-infrared "optical window" of tissue, which is optimal for PTT.[14] The absorption spectrum reverts to that of the non-JAG dye spectrum above the temperature threshold and is reversible.

To test if the feedback mechanism can be tuned to different temperatures, we varied the acyl chain length in the membrane phospholipids: increasing chain length elevates the liquid crystalline-to-fluid phase transition temperature. Each of the dual-chain phospholipids then contained either 14 (DMPC), 16 (DPPC), 17 (DHPC), or 18 (DSPC) carbon atoms. Once synthesized, these NPs were diluted to an optical density of 2 at 824 nm, transferred to 1 cm polystyrene cuvettes and exposed to a collimated 825 nm laser beam at an incident power density of 1.1 $W cm^{-2}$, while monitoring the temperature by thermocouple (Figure 2 A). In all samples, the temperature profile showed a rapid initial increase, followed by a peak and subsequent slow decrease. The peak temperature reached increased with lengthening of the lipid acyl chain, indicating that the temperature set-point could be selected simply by changing the host lipid. Once the temperature set-point was reached, photothermal conversion was inhibited due to the loss of JAG absorption and at this point heat loss from the sample led to a decrease in measured temperature despite continued light irradiance. As negative controls, PEGylated silica-core gold nanoshells (150 nm diameter; peak absorption at $\lambda_{max} = 792$ nm) irradiated under the same conditions did not show any peak in photothermal heating (Figure 2 A).

To check that the observed photothermal response was not due to an irreversible photochemical reaction, such as photobleaching, PEARLs prepared with DPPC were subjected to two cycles of photothermal heating and cooling (Figure S2) and showed repeatable behavior, indicating that the change in photothermal conversion is caused by a physical rather than a photochemical process.

Light transmission at the laser irradiation wavelength during photothermal heating was measured. Photothermal heating resulted in a sigmoidal change in the transmitted light intensity (Figure 2 B). The temperature at the midpoint of the light transmission curve (Figure 2 C) corresponded closely to the peak temperature. Gold

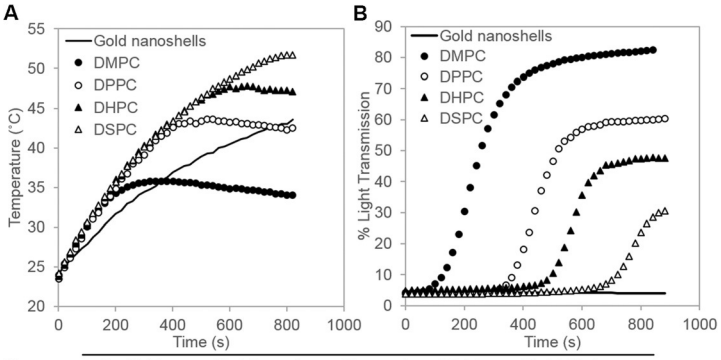

C

Host lipid	Photothermal Heating Max. Temp. (°C)	Temperature at Light Transmission Midpoint (°C)	Host lipid phase transition (°C)[1]
DMPC	36	35	24
DPPC	44	43	41
DHPC	48	47	50
DSPC	52	51	55
Nanoshells	44	n/a	n/a

Figure 2. Thermal (A) and optical (B) time curves during continuous laser irradiation (1.1 $W cm^{-2}$ at 825 nm) of a 1 cm cuvette containing a solution of either PEARLs with different phase-transition temperatures or (control) gold nanoshells. C) Measured maximum and midpoint temperatures achieved during laser irradiation and corresponding phase-transition temperatures of the temperature sensing phospholipid used in each formulation. [1]Host lipid phase transition temperatures as reported in Ref. [17].

nanoshells did not display any measurable change in light transmission under the same conditions (Figure 2B).

To simulate the application of PEARLs within a tissue environment, the NPs were embedded within the rigid matrix of a 3D polyacrylamide (12%) hydrogel phantom and the light propagation through it was measured. Since water movement is impeded by the cross-linked polymer matrix, heat transfer is expected to occur by heat conduction in this material, without significant convective distribution. This recapitulates the properties of NPs dispersed homogeneously through biological tissues (although without the cooling effects of blood perfusion). The phantoms were optically transparent and are stable at temperatures involving photothermal therapy.[15] Cylindrical slabs of polyacrylamide gel (phantoms) were prepared and combined with a solution of NPs prior to polymerization. The concentration of this solution was adjusted to a final optical density of 2.0 at 824 nm. Two other gels were prepared, one embedded with 200 nm polystyrene NPs as a non-absorbing control and the other mixed with non-active PEARLs in which 40 mol% of the phospholipid composition was replaced with cholesterol. Addition of cholesterol affects membrane fluidity and can abolish phase transitions above 33 mol%[16] and when formulated in PEARLs results in the NP behaving as a simple photothermal nanoparticle absorber. The gel phantoms were placed in a custom-built apparatus that enabled simultaneous measurement of light transmission, as well as spatial light distribution and thermographic imaging at an angle perpendicular to the beam path during irradiation with collimated laser light (825 nm; 1.1 $W cm^{-2}$) for 240 s. The results are shown in Figure 3. In the control gel incorporating non-absorbing polystyrene NPs the light penetrating the length of the hydrogel did not change significantly during irradiation (Figure 3A). The corresponding thermographic images showed no change with time, the temperature remaining between 20–25°C throughout the depth of the phantom (Figure 3D). In the phantom containing non-active PEARLs, there was only a slight change in light transmission during irradiation (Figure 3B). Photothermal heating was greatest on the side of the hydrogel facing the laser and a distinct thermal gradient developed, with a difference of approximately 25°C between the hottest region closest to the irradiated face of the phantom and the coolest region at depth (Figure 3E). In contrast, in the phantom incorporating the DPPC PEARLs, the light distribution was initially similar to that with the non-active PEARLs but marked differences were seen after about 30 s, with increased light transmission over time, peaking at around 180 s (Figure 3C). In terms of the spatial distribution of temperature, the phantom reached a maximum temperature of 37°C and displayed only a small

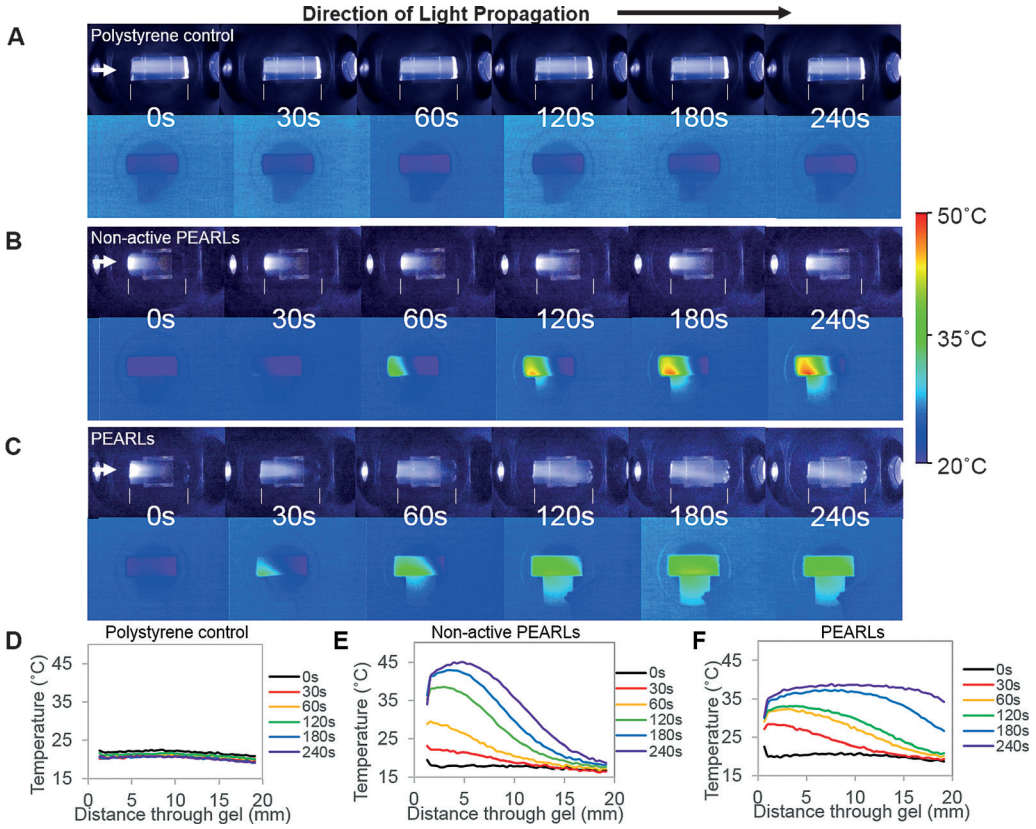

Figure 3. Photothermal heating in 2 cm thick cylindrical hydrogel phantoms containing uniformly dispersed nanoparticles at different time points during continuous irradiation with collimated light (15 $W cm^{-2}$ at 825 nm). In each panel the top images show the light distributions taken with color video camera. The lower images were taken using a calibrated thermal camera for which the temperature scale is shown on the right. Panel (C) shows the PEARLs (prepared with DPPC)-embedded phantoms, while panels (A) and (B) are controls with non-absorbing polystyrene nanoparticles or with the non-active PEARLs, respectively. All phantoms had an initial optical density of 2 at 825 nm. D)–F) Corresponding temperature versus depth profiles through the center of the thermographic images at various times during irradiation.

temperature gradient (ca. 4 °C) between the hottest and coolest areas (Figure 3F). The results from the solution and phantom experiments cannot be directly compared because of differences in experimental setup. The solution experiments utilized an aqueous sample that was insulated within a plastic cuvette and possessed a greater thermal mass than the cylindrical gel phantom. Both of these factors will slow the rate of temperature decrease and thus lead to differing estimates of maximum temperature as observed. Nevertheless, the relative spatial changes in temperature measured in the phantom studies are still valid to demonstrate the heating behavior of DPPC PEARLs compared to the cholesterol-loaded, non-active PEARLs.

Light transmitted through each phantom was measured (Figure 4). The control phantom showed no increase in light transmission over time, while the phantom containing non-active PEARLs showed a slow increase in transmission, up to a factor of 2.6-fold after 240 s. The phantom containing the

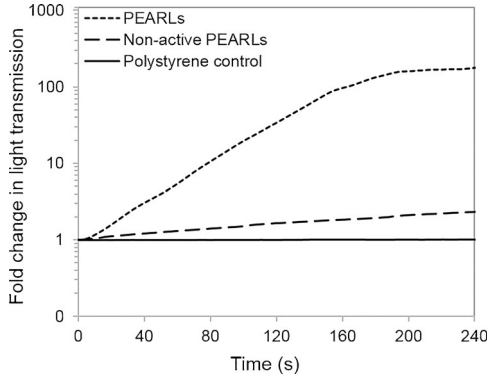

Figure 4. Fold-change in transmitted laser light intensity corresponding to Figure 3.

DPPC PEARLs showed a nearly 200-fold increase in transmission over time. The initial log-linear form of this transmittance curve is as one would expect, with the intensity of light increasing exponentially as an increasing volume of PEARLs switch from an absorbing to non-absorbing mode above the phase transition temperature. Once all the nanoparticles are above the phase-transition temperature throughout the full thickness of the phantom, the transmittance then stabilizes. A limitation of the gel experiments is that the phantoms were essentially purely absorbing in the NIR and the intrinsic absorption and scattering of the gel phantom material itself were minimal. For application of this technology as photothermal enhancers in tissues, there will be additional intrinsic absorption and scattering that will also impact the light attenuation and, hence, the temperature profiles.

In conclusion, we have demonstrated that it is possible to design a photothermal nanoparticle with a closed-loop feedback capability. This feedback mechanism enables an iterative increase in light transmission during photothermal therapy to achieve deeper and more homogeneous heating. This strategy of embedding a negative feedback mechanism into photothermal nanoparticles is a step in the development of adaptive-feedback platforms that may significantly enhance photothermal therapy.

Acknowledgements

This work was supported by the Terry Fox Research Institute (grant no. 1022). Additional support was provided by Prostate Cancer Canada, the Canadian Institutes of Health Research, the Ontario Institute for Cancer Research, the Natural Sciences and Engineering Research Council of Canada, the Canada Foundation for Innovation, and the Tanenbaum Chair in Prostate Cancer Research. We also acknowledge ongoing support from the Princess Margaret Cancer Foundation.

Keywords: feedback mechanisms · J-aggregates · nanoparticles · phase transitions · photothermal therapy

How to cite: *Angew. Chem. Int. Ed.* **2016**, *55*, 10003–10007
Angew. Chem. **2016**, *128*, 10157–10161

[1] a) H.-R. Jiang, N. Yoshinaga, M. Sano, *Phys. Rev. Lett.* **2010**, *105*, 268302; b) R. Luo, J. Wu, N.-D. Dinh, C.-H. Chen, *Adv. Funct. Mater.* **2015**, *25*, 7272—7279; c) K. Okano, A. Nogami, K. Asakura, *Polym. J.* **2014**, *46*, 827–830; d) X. Zhang, Z. Yu, C. Wang, D. Zarrouk, J.-W. T. Seo, J. C. Cheng, A. D. Buchan, K. Takei, Y. Zhao, J. W. Ager, J. Zhang, M. Hettick, M. C. Hersam, A. P. Pisano, R. S. Fearing, A. Javey, *Nat. Commun.* **2014**, *5*, 1–8.
[2] a) Y. Zeng, J. Yao, B. A. Horri, K. Wang, Y. Wu, D. Li, H. Wang, *Energy Environ. Sci.* **2011**, *4*, 4074–4078; b) L. Zhang, B. Tang, J. Wu, R. Li, P. Wang, *Adv. Mater.* **2015**, *27*, 4889–4894.
[3] O. Neumann, A. D. Neumann, E. Silva, C. Ayala-Orozco, S. Tian, P. Nordlander, N. J. Halas, *Nano Lett.* **2015**, *15*, 7880–7885.
[4] a) J.-H. Park, G. von Maltzahn, L. L. Ong, A. Centrone, T. A. Hatton, E. Ruoslahti, S. N. Bhatia, M. J. Sailor, *Adv. Mater.* **2010**, *22*, 880–885; b) J. You, G. Zhang, C. Li, *ACS Nano* **2010**, *4*, 1033–1041.
[5] A. Barhoumi, W. Wang, D. Zurakowski, R. S. Langer, D. S. Kohane, *Nano Lett.* **2014**, *14*, 3697–3701.
[6] a) K. K. Ng, G. Zheng, *Chem. Rev.* **2015**, *115*, 11012–11042; b) I. H. El-Sayed, X. Huang, M. A. El-Sayed, *Cancer Lett.* **2006**, *239*, 129–135; c) L. Cheng, K. Yang, Q. Chen, Z. Liu, *ACS Nano* **2012**, *6*, 5605–5613; d) T. D. MacDonald, T. W. Liu, G. Zheng, *Angew. Chem. Int. Ed.* **2014**, *53*, 6956–6959; *Angew. Chem.* **2014**, *126*, 7076–7079.
[7] S. J. Matcher in *Handbook of Biophotonics*, *Vol. 2* (Eds.: J. Popp, V. V. Tuchin, A. Chiou, S. H. Heinemann), Wiley-VCH, Weinheim, **2011**, p. 448.
[8] C. Sturesson, S. Andersson-Engels, *Med. Phys.* **1997**, *24*, 461–470.
[9] a) O. Raz, M. A. Haider, S. R. H. Davidson, U. Lindner, E. Hlasny, R. Weersink, M. R. Gertner, W. Kucharczyk, S. A. McCluskey, J. Trachtenberg, *Eur. Urol.* **2010**, *58*, 173–177; b) R. J. McNichols, A. Gowda, M. Kangasniemi, J. A. Bankson, R. E. Price, J. D. Hazle, *Lasers Surg. Med.* **2004**, *34*, 48–55.
[10] G. F. Feng, C. Xu, L. Gaoming, Y. Zheng, *Opt. Lett.* **2014**, *40*, 4.
[11] a) E. E. Jelley, *Nature* **1936**, *138*, 1009–1011; b) E. E. Jelley, *Nature* **1937**, *139*, 631–632.
[12] K. K. Ng, M. Shakiba, E. Huynh, R. A. Weersink, Á. Roxin, B. C. Wilson, G. Zheng, *ACS Nano* **2014**, *8*, 8363–8373.
[13] M. Shakiba, K. K. Ng, E. Huynh, H. Chan, D. M. Charron, J. Chen, N. Muhanna, F. S. Foster, B. C. Wilson, G. Zheng, *Nanoscale* **2016**, *8*, 12618–12625.

[14] R. R. Anderson, J. A. Parrish, *J. Invest. Dermatol.* **1981**, *77*, 13 – 19.
[15] a) M. J. Choi, S. R. Guntur, K. I. L. Lee, D. G. Paeng, A. Coleman, *Ultrasound Med. Biol.* **2013**, *39*, 439 – 448; b) L.-S. Bouchard, M. J. Bronskill, *Med. Phys.* **2000**, *27*, 1141 – 1145.
[16] a) B. De Kruyff, P. W. M. Van Dijck, R. A. Demel, A. Schuijff, F. Brants, L. L. M. Van Deenen, *Biochim. Biophys. Acta Biomembr.* **1974**, *356*, 1 – 7; b) R. N. A. H. Lewis, R. N. McElhaney in *The structure of biological membranes*, *2 ed.* (Ed.: P. L. Yeagle), CRC, New York, **2005**, p. 1.
[17] J.R. Silvius in *Lipid-Protein Interactions*, Vol. 2, (Ed.: P.C. Jost and O.H. Griffith), Wiley, New York, **1982**, p. 239.

Received: May 29, 2016
Published online: July 13, 2016

